DR. AUDREY HAY (Orcid ID : 0000-0001-7765-5222)
DR. OLE PAULSEN (Orcid ID : 0000-0002-2258-5455)
DR. VINCENT MAGLOIRE (Orcid ID : 0000-0003-4006-7042)

Article type : Research Report

Submission EJN: Research report

Cholinergic modulation of Up-Down states in the mouse medial entorhinal cortex *in vitro*

Running title: Acetylcholine reorganises network activity

Y Audrey Hay[1,*], Przemyslaw Jarzebowski[1,*], Yu Zhang[1,*], Richard Digby[1], Viktoria Brendel[1], Ole Paulsen[1], Vincent Magloire[1,2]

Affiliations:

1. Department of Physiology, Development and Neuroscience, Physiological Laboratory, University of Cambridge, Cambridge, United Kingdom.
2. UCL Queen Square Institute of Neurology, University College London, London, United Kingdom.

*Contributed equally to the work.

Corresponding authors:

This article has been accepted for publication and undergone full peer review but has not been through the copyediting, typesetting, pagination and proofreading process, which may lead to differences between this version and the Version of Record. Please cite this article as doi: 10.1111/ejn.15032

Ole Paulsen: op210@cam.ac.uk and Vincent Magloire: v.magloire@ucl.ac.uk

Number of pages: 34

Number of figures: 8 plus 2 supplementary figures

Number of words: Abstract: 225

Whole manuscript: 6656

Keywords:

Acetylcholine
Network synchrony
Population calcium imaging
Slow wave sleep
Spontaneous activity

Abstract

Cholinergic tone is high during wake and rapid eye movement sleep and lower during slow wave sleep (SWS). Nevertheless, the low tone of acetylcholine during SWS modulates sharp wave ripple incidence in the hippocampus and slow wave activity in the neocortex. Linking the hippocampus and neocortex, the medial entorhinal cortex (mEC) regulates the coupling between these structures during SWS, alternating between silent Down states and active Up states, which outlast neocortical ones. Here, we investigated how low physiological concentrations of acetylcholine (ACh; 100-500 nM) modulate Up and Down states in a mEC slice preparation. We find that ACh has a dual effect on mEC activity: it prolongs apparent Up state duration as recorded in individual cells and decreases the total synaptic charge transfer, without affecting the duration of detectable synaptic activity. The overall outcome of ACh application is excitatory and we show that ACh increases Up state incidence via muscarinic receptor activation. The mean firing rate of principal neurons increased in around half of the cells while the other half showed a decrease in firing rate. Using two-photon calcium imaging of population activity, we found that population-wide network events are more frequent and rhythmic during ACh and confirmed that ACh modulates cell participation in these network events, consistent with a role for cholinergic modulation in regulating information flow between the hippocampus and neocortex during SWS.

Introduction

Acetylcholine (ACh) is a key neuromodulator that strongly influences cortical network activity. The cortical ACh concentration is high during wake and rapid eye movement (REM) sleep and lower during slow wave sleep (SWS), when basal forebrain cholinergic neurons still discharge at around 1 Hz, maintaining a low cholinergic tone (Kametani & Kawamura, 1990; Marrosu *et al.*, 1995; Lee *et al.*, 2005; Mena-Segovia *et al.*, 2008). SWS is characterised by a cortical slow oscillation (<1 Hz) consisting of synchronous membrane potential fluctuations between a depolarized ('Up') and hyperpolarized ('Down') state (Steriade, Nunez, *et al.*, 1993). Neocortical Up states in anaesthetised mice are dependent on muscarinic ACh receptors (Lőrincz *et al.*, 2015), and pharmacological reinstatement of a low cholinergic tone in neocortical slices induces rhythmic Up and Down states with properties similar to those observed during the slow oscillation *in vivo*, consistent with a low cholinergic tone during SWS (Carracedo *et al.*, 2013; Lőrincz *et al.*, 2015).

The medial entorhinal cortex (mEC) is the main gateway between the neocortex and the hippocampus (Strien *et al.*, 2009). During SWS, the mEC is suggested to modulate cortico-hippocampal interactions because mEC Up states outlast and bridge between consecutive neocortical Up states (Hahn *et al.*, 2012). Slices from the mEC show spontaneous long-duration Up states (Mann *et al.*, 2009), reminiscent of those seen *in vivo*, mediated by kainate receptors (Digby *et al.*, 2017). The mEC is highly sensitive to cholinergic modulation (Klink & Alonso, 1997; Egorov *et al.*, 2002; Steriade, 2004; Fransén *et al.*, 2006; Zhang *et al.*, 2011; Jochems *et al.*, 2013), which raises the question of how a low cholinergic tone modulates the spontaneous slow oscillation in the mEC.

We addressed this question using a slice preparation of the juvenile mouse mEC, which shows spontaneous Up-Down states when superfused with a solution containing 1 mM Mg^{2+} and 1.2 mM Ca^{2+} (Mann *et al.*, 2009). We recorded Up and Down state activity using dual intra- and extracellular electrodes and two-photon calcium imaging of population activity. Using whole-cell recording, we show that a low physiological concentration of ACh (100-500 nM; Kametani & Kawamura, 1990; Marrosu *et al.*, 1995) increases Up state duration and incidence via muscarinic receptor activation, while maintaining the balance of excitatory and inhibitory recurrent synaptic transmission. Using calcium imaging, we find that ACh increases the duration, frequency, and rhythmic occurrence of population-wide Up states and that ACh modulates the participation of neurons in these Up-state events. These results suggest an important role for cholinergic input in modulating Up-Down states in the medial entorhinal cortex.

Materials and Methods:

Animals: All experiments were conducted in accordance with the UK Animals (Scientific Procedures) Act (1986) following ethical review by the University of Cambridge Animal Welfare and Ethical Review Body (AWERB). All animal procedures were authorised under Personal and Project licenses held by the authors. Animals were housed in conventional cages, on a 12h/12h light/dark cycle, with *ad libitum* access to food and water. Electrophysiological experiments were performed on *C57BL/6* (Harlan, Bicester, UK) mice of both sexes. For calcium imaging recordings, we used either heterozygous Thy1-GCaMP6f transgenic mice (Jax: 024276; Dana *et al.*, 2014) or homozygous GCaMP6f-floxed mice (Jax: 024105; Madisen *et al.*, 2015) crossed with heterozygous Necab1-cre mice, which express the Cre recombinase in the thalamus as well as in excitatory neurons in the cortex (Phillips *et al.*, 2019). Necab1-cre mice were made in the Janelia Transgenic Mouse Core (https://www.janelia.org/support-team/gene-targeting-and-transgenics) and provided prepublication by the Hantman and Dudman laboratories.

Slice preparation: Horizontal slices (400 µm) through the hippocampus-medial entorhinal cortex were prepared from both sexes on postnatal day (P)14 to P19 between one and three hours into the light phase of the light/dark cycle as previously described (Mann *et al.*, 2009; Craig *et al.*, 2012). Briefly, decapitation was performed under deep isoflurane-induced anesthesia and, after removal of the skull, the brain was submerged in ice-cold (≤4 ^{0}C) standard artificial cerebrospinal fluid (aCSF) containing (in mM): NaCl (126), KCl (3.5), NaH_2PO_4 (1.25), $MgSO_4$ (2), $CaCl_2$ (2), $NaHCO_3$ (26), and glucose (10), pH 7.2-7.4 for 1-2 min. Slices were then cut using a vibrating blade microtome (Leica, VT 1200 S, Germany) and transferred to an interface chamber between humidified carbogen gas (95% O_2, 5% CO_2) and modified artificial CSF (aCSF) with reduced $MgSO_4$ (1 mM) and $CaCl_2$ (1.2 mM). Slices were maintained in interface condition prior to recordings.

Electrophysiology: Slices were mounted on coverslips coated with 0.1% poly-L-lysine in ultrapure H_2O (Sigma-Aldrich) and transferred to a submerged-style recording chamber perfused with modified aCSF at 4-5 mL·min^{-1} at 30-32 ^{0}C to promote spontaneous persistent network activity (Hájos *et al.*, 2009). Whole-cell patch-clamp recordings were performed on mEC neurons with glass pipettes pulled from standard borosilicate glass tubing containing (in mM): K-gluconate (110), Hepes (40), ATP-Mg (2), GTP (0.3), and NaCl (4) with a resistance of 4-6 MΩ for current

clamp recordings and Cs-methylsulfonate (120), Hepes (10), EGTA (0.2), ATP-Mg (4), GTP(0.3), QX-314 (10), and CsCl (20) with a resistance of 3-4 MΩ for voltage clamp recordings. Both pipette solutions were adjusted to obtain a pH of 7.2–7.3 at 25 ^{0}C and an osmolarity between 275 and 290 mosmol·L^{-1}. In addition, we performed cell-attached recordings in loose-seal configuration (≤40 MΩ) using pipettes of 3-5 MΩ filled with aCSF. For current clamp experiments, cells exhibiting membrane potential positive to -55 mV were discarded. In addition, series resistance was monitored throughout the experiment. Cells were rejected if the series resistance was above 20 MΩ and/or if the change in series resistance in control condition versus drug was higher than 20% for voltage clamp experiments. No series resistance compensation or liquid junction potential correction was applied.

Electrophysiology analysis: All data were acquired using an AXON Multiclamp 700B amplifier (Molecular Devices, Sunnyvale, CA, USA), low-pass filtered at 2 kHz, and digitized at 5 kHz using an Instrutech ITC-18 and Igor Pro (WaveMetrics) custom-made acquisition procedures. Automatic off-line detection of Up and Down state transitions was performed using custom-made procedures in Igor Pro as described previously (Craig *et al.*, 2012). Briefly, during Up states, the membrane potential noise increases due to synaptic activity. We calculated the product of the ratio of the root mean square of the membrane potential in two successive analysis windows each containing 120 data points (24 ms at 5 kHz) and the ratio of the relative change in membrane potential between the current and the antepenultimate time window. Any change of more than 10% was considered as a Down-to-Up or Up-to-Down state transition. All traces were visually inspected to confirm the detection of appropriate Up and Down state transitions. The spike frequency was measured over the duration of detected Up or Down state periods.

Calcium imaging: As for the electrophysiological experiments, slices were mounted on coverslips coated with 0.1% poly-L-lysine and transferred to a submerged-style recording chamber perfused with modified aCSF at 4-5 mL·min^{-1} at 30-32 ^{0}C. Population imaging was done with a two-photon microscope (VIVO, 3i systems). Two-photon excitation was performed using a MaiTai Ti-Sapphire laser (Spectra-physics, Inc.) at 890 nm, coupled to a galvanometer scanning unit that was mounted on a Zeiss AxioExaminer Z1 upright microscope equipped with a 20x/1.0 NA objective. Fluorescence was acquired using non-descanned GaAsP detectors behind the objective. Recordings were performed with a 300 um x 300 um field of view (FOV), at an acquisition rate of 1-3 Hz. One, two, or three z-planes were recorded for 10-27 min per condition; for the analysis, only the z-plane with the highest number of cells was used.

Calcium data processing: To extract the calcium fluorescence signal, the raw fluorescence movies were analysed with Suite 2P (Pachitariu *et al.*, 2017). This software automates analysis by performing the following steps: First, x-y drift is corrected by aligning the frames, second, regions of interests (ROIs) are defined, and, third, the fluorescence signal is extracted. ROIs are identified by clustering together neighboring pixels based on the correlation of their activity and a spatial mask is generated with pixels weighted in proportion to their correlation with the ROI's peak correlation. The detected ROIs were manually reviewed to include only those with spatial mask overlying cell bodies identified by their shape and visible nucleus in the time-averaged movie. Finally, Suite 2P extracts the fluorescence signal from each ROI based on a model assuming that the fluorescence has two sources: the cell and the out-of-focus fluorescence from the neuropil. As a result, the neuronal fluorescence signal used for analysis excludes the neuropil fluorescence.

Analysis of calcium signal: To calculate neuronal fluorescence changes, first, the detrended baseline fluorescence $F_0(t)$ was calculated using a locally estimated scatterplot smoothing (LOESS) algorithm. This algorithm works as a low pass filter, adapting the calculated baseline fluorescence to reflect slow fluctuations in the signal caused by effects such as photobleaching. The neuronal fluorescence change was calculated as $\Delta F/F_0(t) = (F(t)-F_0(t))/F_0(t)$, where $F(t)$ was the fluorescence signal at time t. The statistical analysis was performed on z-scored $\Delta F/F_0$ values (i.e. mean subtracted and divided by the standard deviation (s.d.)). We identified calcium events when the neuronal z-scored signal exceeded a threshold of 4 s.d. and had a prominent peak exceeding the neighboring local minimum by more than 4 s.d. A cell was identified as active if it was found to have a calcium event in any of the three recording conditions. The duration of the event was defined as the time between upward and downward crossing of the threshold value. Slices with at least 65% of their cells active were included in the analysis (5 out of 13 slices from Necab1-cre*GCaMP6f-floxed mice, all slices from Thy1-GCaMP6f mice). We cropped the recordings to equal length of 7 minutes.

Population events: Population events were detected by analysing the population mean of the z-scored and time-binned signal. First, for each cell the mean z-score was calculated during each one-second-long bin. Next, the values for each time bin were averaged across the cells for each slice. Population events were detected when the local maximum of the signal crossed a set threshold. The threshold was manually adjusted for each slice to capture the peaks. If multiple local maxima were detected within a single period during which the z-score exceeded 50% of the threshold value, only the peak with the highest value was included. A neuron was deemed to participate in the population event if it had a z-score value exceeding half of the population event

threshold. The duration of a population event was defined as the time between upward and downward crossing of 50% of the peak value. For a cell to be considered to participate in population events, it had to be active in 70% of the detected population events. The choice of the threshold did not affect the significance of the effects and was tested for the minimum level of participation set at 50, 60, 70 and 80%.

Statistical analysis: The statistics for electrophysiology experiments were performed using Prism 5 (GraphPad Software Inc.) and R (https://www.r-project.org). Non-parametric tests were used throughout the study. Comparison between paired data sets was performed using Wilcoxon signed-rank test. One-way ANOVA on ranks was done using Kruskal-Wallis test, and two-way ANOVA on ranks (ART ANOVA) was done using standard ANOVA after data alignment and ranking using ARTool package in R. Data are reported as mean ± S.E.M. unless stated otherwise.

Statistical analysis of the calcium imaging data was performed using MATLAB and R. For statistical testing of the autocorrelations, we assumed a normal distribution of the signal values and applied Bartlett's formula for the estimate of the standard error. Bartlett's formula assumes that the random time series is generated by a moving average process where two sequential observations are correlated. Standard error was calculated as:

$$SE(k) = \sqrt{1 + 2\Sigma_{i=1}^{k-1} r_i^2 / N}$$

where k is the lag, r_i is the autocorrelation at lag i and N is the number of observations in the recording. The non-zero-lag peak value r_k of the autocorrelation was tested for the null hypothesis that the real autocorrelation value is not different from 0. The autocorrelation is said to be significant if the r_k / *SE(k)* ratio was outside of the 0.95 quantile of the *Norm(0, 1)* distribution.

Code and data accessibility: Code used for the analysis of electrophysiological and calcium imaging data and to generate the figures can be accessed on the authors' GitHub site: https://github.com/przemyslawj/ento_ach_caimg. Electrophysiological and calcium imaging data will be shared on any reasonable request.

Drugs: Acetylcholine (Sigma-Aldrich) stock solution was made daily at an initial concentration of 5 mM and then diluted in aCSF to a final concentration of 100-500 nM. Atropine, pirenzepine AFDX-116 and mecamylamine were purchased from Tocris.

Results

Low physiological concentrations of ACh increase Up state duration and occurrence via muscarinic receptor activation

We monitored Up and Down state activity in spontaneously active slices of the mEC of juvenile mice (n = 40 animals aged P14-P19) using whole-cell current-clamp recordings from individual layer II-III principal neurons (n = 60). Previous reports indicate that cortical extracellular ACh concentration varies between 50 nM and 5 µM depending on the behavioral state (Kametani & Kawamura, 1990; Marrosu *et al.*, 1995; Hasselmo & McGaughy, 2004; Parikh *et al.*, 2007; Zhang *et al.*, 2010). We investigated how low physiological concentrations of bath applied ACh (100-500 nM), consistent with values measured during SWS (Kametani & Kawamura, 1990; Marrosu *et al.*, 1995), influence Up and Down state activity. Bath application of 100-500 nM ACh induced an increase in Up state duration and incidence (Up state duration: Ctrl, 2.75 ± 0.20 s vs ACh, 4.50 ± 0.39 s; Wilcoxon signed-rank test, W = 29; n = 40; $p < 5.10^{-9}$; Incidence: Ctrl, 3.26 ± 0.39 vs ACh, 6.19 ± 0.48 min^{-1}; W = 29; n = 40; $p < 6.10^{-7}$; Figure 1A,B, S1-1A). We did not detect a significant difference between different ACh concentrations in this concentration range (Ratio of duration relative to baseline: 100 nM, 1.89 ± 0.77, n = 5; 200 nM, 1.50 ± 0.08, n = 4; 300 nM, 1.64 ± 0.15, n = 3; 400 nM, 1.92 ± 0.61; n = 2; 500 nM, 1.80 ± 0.31, n = 8; Kruskal-Wallis test, p = 0.83; Figure S1-1C; Ratio of incidence relative to baseline: 100 nM, 1.99 ± 0.59, n = 5; 200 nM, 2.04 ± 0.35, n = 4; 300 nM, 1.60 ± 0.13, n = 3; 400 nM, 1.35 ± 0.50; n = 2; 500 nM, 5.60 ± 1.70, n = 8; Kruskal-Wallis test, p = 0.14; Figure S1-1D). Thus, low concentrations of ACh modulate Up state incidence and duration. In the presence of a higher concentration of ACh (5 µM), Up and Down states were abolished and a periodic variation of the membrane potential was seen in 5 out of 7 neurons (Figure S1-1A,B) similar to the intrinsic voltage-dependent oscillations previously observed in mEC stellate cells (Dickson *et al.*, 2000). Washing out ACh (5 µM) restored Up and Down states, but the incidence and Up state morphology remained affected even after 30 minutes of wash-out (n = 2; Figure S1-1A).

We next asked which receptors mediate ACh modulation of Up states. Cholinergic effects are mediated through ionotropic nicotinic receptors and metabotropic muscarinic receptors. The ACh-induced (250-500 nM) increase in Up state duration and incidence was reversed by application of atropine (Atr; 1 µM), a muscarinic receptor antagonist (Duration: ACh, 3.89 ± 0.5 s vs Atr, 2.90 ± 0.26 s; Wilcoxon signed-rank test, W = 60; n = 11; p = 0.014; Incidence: ACh, 7.38 ± 0.82 min^{-1} vs Atr, 2.80 ± 0.40 min^{-1}; Wilcoxon signed-rank test, W = 66, n = 11, p = 0.001; Figure 1A,B). Application of atropine alone did not affect the duration and incidence of Up states but prevented

the ACh-induced modulation (Duration: Ctrl, 2.93 ± 0.62 s, Atr, 2.54 ± 0.22 s, Atr+ACh, 2.51 ± 0.21 s; Kruskal-Wallis test, n = 7, p = 0.96; Incidence: Ctrl, 4.01 ± 1.13 min^{-1}, Atr, 4.06 ± 1.28 min^{-1} vs Atr+ACh, 4.5 ± 1.07 min^{-1}; Kruskal-Wallis test, n = 7, p = 0.90; Figure 1C). In contrast, bath application of the nicotinic receptor antagonist mecamylamine (Mec; 10 µM) did not change the duration of Up states when co-applied after ACh (ACh, 5.67 ± 0.8 s vs Mec+ACh, 6.52 ± 0.97 s; Wilcoxon signed-rank test, W = 11; n = 9; p = 0.20; Figure 1D,E), nor their incidence (ACh, 2.71 ± 0.29 min^{-1} vs Mec+ACh, 2.66 ± 0.27 min^{-1}; Wilcoxon signed-rank test, W = 25.5; n = 9; p = 0.77; Figure 1D,E) and bathing of mecamylamine prior to ACh did not prevent ACh-induced modulation of Up states (Duration: Ctrl, 6.41 ± 1.47 s, Mec, 5.73 ± 0.95 s, Mec+ACh, 15.83 ± 3.38 s; Kruskal-Wallis test, n = 7, p = 0.027; Incidence: Ctrl, 1.79 ± 0.31 min^{-1}, Mec, 1.54 ± 0.29 min^{-1} vs Mec+ACh, 2.4 ± 0.27 min^{-1}; Kruskal-Wallis test, n = 7, p = 0.09; Figure 1F). Thus, Up and Down state modulation by a low concentration of ACh is mediated primarily by muscarinic receptor activation.

Subtypes of muscarinic receptors mediating ACh modulation of Up and Down states

We next asked which subtypes of muscarinic receptors are involved in the modulation of Up and Down states. The muscarinic receptor family consists of 5 subtypes of receptor (M1-M5) differentially distributed in the cortex. M1/M3 subtypes are localised mainly on pyramidal neurons whereas M2/M4 are predominantly found presynaptically at inhibitory synapses (Levey, 1996; Lucas-Meunier *et al.*, 2003; Chaudhuri *et al.*, 2005; Bubser *et al.*, 2012). Co-application of ACh with the selective M1/M3 muscarinic antagonist pirenzepine (Pir; 10 µM) entirely reversed ACh modulation of duration and incidence of Up states (Duration: ACh, 4.13 ± 0.76 s vs Pir 2.60 ± 0.25 s; Wilcoxon signed-rank test, W = 28; n = 7; p = 0.02; Incidence: ACh, 8.1 ± 0.79 min^{-1} vs Pir, 2.61 ± 0.66 min^{-1}; Wilcoxon signed-rank test, W = 28, n = 7, p = 0.02; Figure 2A,B) and application of Pirenzepine prior to ACh prevented ACh-induced modulation of Up states (Duration: Ctrl, 3.35 ± 0.6 s, Pir, 3.51 ± 0.71 s, Pir+ACh, 3.25 ± 0.79 s; Kruskal-Wallis test, n = 6, p = 0.72; Incidence: Ctrl, 3.43 ± 0.86 min^{-1}, Pir, 3.33 ± 0.63 min^{-1} vs Pir+ACh, 3.9 ± 0.42 min^{-1}; Kruskal-Wallis test, n = 6, p = 0.84; Figure 2C). Application of AFDX-116 (1 µM), an M2/M4 antagonist, did not significantly affect the duration of Up states (Duration: ACh, 4.41 ± 0.43 s vs AFDX 3.61 ± 0.46 s; Wilcoxon signed-rank test, W = 24; n = 7; p = 0.11), but the incidence was significantly reduced (Incidence: ACh, 6.8 ± 0.39 min-1 vs AFDX, 4.04 ± 0.89 min-1; Wilcoxon signed-rank test, W = 28, n = 7, p = 0.016; Figure 2D,E), suggesting that M2/M4 muscarinic receptors also contribute to the cholinergic modulation of Up states. However, AFDX-116 application prior to ACh application did not prevent ACh-induced modulation of Up state duration

or incidence (Duration: Ctrl, 3.44 ± 0.47 s, AFDX, 3.33 ± 0.26 s, AFDX+ACh, 5.80 ± 1.37 s; Kruskal-Wallis test, n = 9, p = 0.02; Incidence: Ctrl, 2.26 ± 0.36 min^{-1}, AFDX, 2.66 ± 0.46 min^{-1} vs AFDX+ACh, 5.01 ± 0.69 min^{-1}; Kruskal-Wallis test, n = 9, p = 0.18; Figure 2F). Thus, the cholinergic modulation of Up state activity in mEC principal neurons is mediated primarily by M1/M3 muscarinic receptors with a possible additional contribution from M2/M4 muscarinic receptors.

ACh reduces both excitatory and inhibitory charge transfer without affecting E/I balance

To better understand how ACh application modulates synaptic transmission during Up states, we measured the excitatory and inhibitory synaptic inputs that mEC neurons receive during synaptic Up states. We monitored excitatory synaptic currents by voltage-clamping the cell at a holding potential of -70 mV while we sampled inhibitory currents at a holding potential of +10 mV. During Up states, the excitation/inhibition (E/I) ratio was well balanced (1.19 ± 0.16) with an average excitatory charge transfer of -1.01 ± 0.12 nC and an inhibitory one of 0.88 ± 0.07 nC (n = 9; Figure 3A,B). ACh (250-500nM) did not significantly change the E/I ratio (1.30 ± 0.22; Wilcoxon signed-rank test, W = 1, n = 9, p =1, Figure 3C) but proportionally reduced both excitatory and inhibitory charge transfer by more than 30% (E, -0.62 ± 0.06 nC; Wilcoxon signed-rank test, W = 1, n = 9, p = 0.008, and I, 0.58 ± 0.09 nC; W = 40.5, n = 9, p = 0.038, Figure 3B). We asked whether a reduction of the membrane resistance during ACh could account for the reduction of charge transfer. However, we did not observe any significant change of resistance either at -70 mV or +10 mV between control and ACh conditions (Rm -70 mV: Ctrl, 333.2 ± 36.7 MΩ vs ACh, 340.4 ± 33.8 MΩ; Wilcoxon signed-rank test, W = 21, n = 9, p = 0.91; Rm +10 mV: Ctrl, 145.7 ± 10.2 MΩ vs ACh, 160.2 ± 11.4 MΩ; W = 8, n = 9, p = 0.098; Figure 3D). Surprisingly, the total duration of excitatory and inhibitory "Up state" currents was not affected by ACh (E: Ctrl, 3.18 ± 0.32 s vs ACh, 2.76 ± 0.25 s; Wilcoxon signed-rank test, W = 26, n = 9, p = 0.73; I: Ctrl, 2.82 ± 0.24 s vs ACh, 2.45 ± 0.21 s; W = 29, n = 9, p = 0.50; Figure 3E) in spite of the lengthening of Up states as recorded in individual neurons in current clamp mode (Figure 1).

ACh increases overall firing frequency and differentially modulates spiking activity between states and neurons

We next investigated the effect of a low concentration of ACh on the firing pattern of individual neurons by performing cell-attached recordings in loose patch configuration, a method that

allowed us to observe spiking behaviour with minimal disturbance of the recorded cells (Alcami *et al.*, 2012). Network activity was simultaneously monitored using voltage-clamp recording of a close-by cell to detect synaptic activity corresponding to the Up state (Figure 4A). Down state was defined by default as the period between synaptic Up states. Overall spiking activity significantly increased after bath application of ACh (250-500nM; Ctrl, 1.43 ± 0.27 Hz; ACh, 3.55 ± 0.82 Hz; Wilcoxon signed-rank test, W = 50, n = 25, p = 0.0016; Figure 4A-E). Further analysis revealed that the firing frequency and spike count increased during Down states (Frequency: Ctrl, 0.35 ± 0.16 Hz; ACh, 2.12 ± 0.80 Hz; Wilcoxon signed-rank test, W = 28, n = 25, p = 0.007; Count: Ctrl, 1.8 ± 0.7 spikes; ACh, 8.8 ± 3.1 spikes, W = 34, p = 0.015; Figure 4Fi) and remained stable during Up states (Frequency: Ctrl, 5.47 ± 0.88 Hz vs ACh, 5.76 ± 1.04 Hz; Wilcoxon signed-rank test, W = 133, n = 25, p = 0.44; Count: Ctrl, 12.6 ± 1.9 spikes; ACh, 13.4 ± 2.2 spikes, W = 143, p = 0.62; Figure 4Fii). This effect was prevented by the muscarinic receptor antagonist atropine (Mean firing frequency: Atr, 0.82 ± 0.15 Hz vs Atr +ACh, 0.73 ± 0.17 Hz; Wilcoxon signed-rank test, W = 23.5, n = 8, p = 0.48; Down state firing frequency: Atr, 0.16 ± 0.05 Hz vs Atr + ACh, 0.30 ± 0.17 Hz; W = 10, n = 8, p = 0.55; Up state firing frequency: Atr, 4.23 ± 0.62 Hz vs Atr + ACh, 4.68 ± 0.95 Hz; W = 11, n = 8, p = 0.38; not shown). Analysis of the spiking behaviour of individual cells during Up states revealed that 50% of the recorded neurons (12 out of 24) increased their spiking frequency during Up and Down states in the presence of ACh (Figure 4A,B,G). The other cells (12 out of 24) showed an overall decrease in their spiking activity in the presence of ACh (Figure 4C,D,G). We asked whether ACh reorganises the spike distribution during the Up state by quantifying the number of spikes occurring during the first or second half of the Up state. In control condition, neurons fired primarily during the first half (Count Ctrl: 0-50%, 10.1 + 1.6 spikes, 50-100%, 4.7 ± 1.0 spikes; Wilcoxon signed-rank test, W = 322, n = 25, p < 10-6), with 72.2 ± 2.5% of the spikes detected. ACh application did not significantly affect the distribution (Count ACh: 0-50%, 11.1 + 2.1 spikes, 50-100%, 7.1 ± 1.9 spikes; two-way ART ANOVA, 0-50% vs 50-100% p = 0.001, Ctrl vs ACh p = 0.83), with 69.8 ± 3.7% of spikes emitted during the first half of the Up state (Figure 4H). Finally, we asked whether the location of the neurons influenced their response to ACh and observed that the proportion of neurons from layer III showing an overall increase in firing frequency during Up state was significantly higher than the proportion of neurons from layer II (Layer II, n = 2/11 neurons; Layer III, n = 9/13 neurons; two proportion z-test, p = 0.01; Figure 4I). Altogether these results indicate that a low tone of ACh reorganises network activity by activating some neurons while suppressing others without modifying the spike distribution over Up states.

Electrophysiological Up states are correlated with peaks of population calcium signals

In order to observe the effect of ACh simultaneously in a larger sample of cells, we used single-cell resolution two-photon calcium imaging in layers II-III of the mEC. We used two different strains of mice expressing the genetically encoded calcium indicator GCaMP6f: Necab-Cre*GCaMP6f-floxed (Necab1*GCaMP6f) expressing GCaMP6f in excitatory cells, and Thy1-GCaMP6f sparsely expressing GCaMP6f in excitatory layer II/III and layer V cells (Figure 5A). We first examined the relationship between Up states and calcium events by simultaneously recording one cell in current-clamp mode while monitoring the calcium signal of surrounding neurons (Figure 5B-C). The fluorescence traces of the active cells were positively correlated with the membrane potential of the patched cell in both the control and ACh condition (Ctrl: 0.21 ± 0.05, median 0.23, n = 9 neurons from 3 slices; ACh: 0.32 ± 0.04, median 0.39, n = 27 neurons from 3 slices, Figure 5D). To find the temporal relation between the two signals, we cross-correlated the electrophysiological trace of the patched cell with the calcium signal of individual imaged cells (n = 3 slices from 2 animals). The cross-correlation values peaked at near zero second lag (Ctrl: -0.83 s ± 0.68 s, median 0 s, n = 9; ACh: 0.23 ± 0.47 s, median 0.33 s, n = 27), suggesting that the Up state observed in the patched cell and the increased calcium fluorescence in the other cells represent the same network-wide event.

ACh enhances synchronous rhythmic activity and modulates cell recruitment during population events

We identified and extracted the calcium signal of between 32 and 110 cells per slice (Figure 6A-C and Figure S6-1). Only slices showing transient calcium events in control condition were included in the final analysis (n = 11 animals: 5 Necab1*GCaMP6f and 6 Thy1-GCaMP6f animals; see Methods for the detection of transient calcium events). Recordings from the Thy1-GCaMP6f and the Necab1*GCaMP6f animals were pooled together as we did not find any differences between the mouse lines in the detected transient calcium events: the median event frequency for a cell was similar in the control condition (Necab1*GCaMP6f: 0.30 ± 0.06 min^{-1} (n = 5) and Thy1-GCaMP6f: 0.44 ± 0.09 min^{-1} (n = 6); Wilcoxon rank-sum test, W = 9, p = 0.3) and so was the median event duration (Necab1*GCaMP6f: 3.0 ± 1.0 s (n = 5) and Thy1-GCaMP6f: 2.9 ± 0.3 s (n = 6); Wilcoxon rank-sum test, W = 9, p = 0.3; see all recordings in Figure S6-1).

We defined population events in the time-binned signal as events in which the mean z-score crossed a manually adjusted threshold (Figure 6A). After adding ACh (250 nM) to the

superfusate, the duration of population events significantly increased from 2.2 ± 0.3 s to 4.0 ± 0.6 s (Wilcoxon signed-rank test on median event durations, W = 45, n = 10, p = 0.008; Figure 6B) as well as their incidence from 1.4 ± 0.2 to 3.2 ± 0.3 min^{-1} (Wilcoxon signed rank test on event frequencies, W = 52, n = 10, p = 0.006; Figure 6C). This effect was reversed by co-application of atropine with ACh: event duration significantly decreased from 4.0 ± 0.6 s to 2.0 ± 0.3 s (Wilcoxon signed-rank test on median event durations, W = 45, n = 10, p = 0.008; Figure 6B), and the incidence decreased from 3.2 ± 0.3 to 1.3 ± 0.2 min^{-1} (Wilcoxon signed-rank test on event frequencies, W = 55, n = 10, p = 0.002; Figure 6C). In addition, the $\Delta F/F_0$ amplitude of the population event peaks significantly increased between the control and ACh condition from 0.14 ± 0.02 to 0.27 ± 0.04 (Wilcoxon signed-rank test on median peak ΔF/F values, W = 35, n = 10, p = 0.04; Figure 6D) but did not significantly decrease following the addition of atropine (Wilcoxon signed-rank on median peak $\Delta F/F_0$ values, W = 24, n = 10, p = 0.24; Figure 6D). The increased frequency, duration and amplitude of population events were accompanied by an increase in the median frequency and duration of transient calcium events in individual cells (frequency: median increased from 0.4 ± 0.1 min-1 to 1.5 ± 0.3 min-1; Wilcoxon signed-rank test on median event frequency in each slice, W = 54, n = 10, p = 0.008; Figure 6E; duration: median increased from 2.1 ± 0.3 to 3.3 ± 0.5 s; Wilcoxon signed-rank test on median duration in each slice, W = 36, n = 10, p = 0.01; Figure 6F). Hence, the ACh effect on population event duration and incidence observed here is similar to the electrophysiological data.

Plots of population activity in ACh (Figure 6A) revealed a periodicity of the network activity, which we quantified by calculating the autocorrelation function (Figure 7A). We observed an increase in autocorrelation peaks in the presence of ACh (8 out of 11 slices showed significant non-zero-lag peaks in the autocorrelogram) compared to control condition (3 out of 11 slices showed significant autocorrelation peaks) and atropine condition (only 1 of the 11 slices showed significant autocorrelation peaks; Figure 7B). The average lag of the first non-zero-lag peak in the autocorrelation in the ACh condition was 17 s (SD = 5.1 s, n = 8) with a peak value of 0.52 (SD = 0.26, n = 8; Figure 7C).

Next, we looked at how the ACh and ACh + atropine conditions affected the recruitment of cells during population events. In the analysis, we included 9 slices with more than one population event in each of the three conditions. The population events reliably recruited a large part of the network (Figure 6A): 61 ± 7% cells participated in ≥ 70% of population events during the control and 73 ± 8% of cells during the ACh condition (Wilcoxon signed-rank test on median count of cells participating in more than 70% of events, W = 31, n = 9, p = 0.07 two-tailed; Figure 8A). We assessed if the stability of cell assemblies was modulated by ACh by monitoring whether the cells

that changed their participation from active to non-active and from non-active to active, returned to their previous state after application of atropine. We assessed the significance of this pattern by comparing it with a model of random reassignments. In the random model, each cell in the network had an equal probability of switching from active to non-active and vice-versa. We set the probability of the switch equal to the proportion of cells empirically observed to switch their participation. We simulated 1000 random reassignments governed by the experimentally calculated probabilities. The number of cells that followed a pattern of temporal switch controlled by ACh and reversed by atropine was significantly higher in 6 out of 9 slices compared to the simulated random reassignments ($p < 0.05$) and when tested on cells from all slices pulled together ($p < 0.01$; Figure 8B).

Hence, consistent with our intracellular recordings, these calcium imaging results show that ACh induces an increase in co-activity in the network through rhythmic population events of increased frequency and duration. Moreover, the neuronal pattern of activation appeared stable during population-wide bursts while ACh reversibly modulated individual cell recruitment during these events.

Discussion

We have examined how a low physiological concentration of ACh, similar to the estimated concentration during SWS, affects Up and Down state activity in acute slices of the mEC. We found that ACh increases the duration and incidence of Up states in layer II/III principal neurons via muscarinic receptor activation. Moreover, ACh reduces both excitatory and inhibitory recurrent synaptic transmission and causes ~50% of the neurons to increase their firing in Down states and ~50% to decrease their firing in Up states. Finally, at population level, we found that ACh promotes the synchronisation of mEC neurons and reorganises patterns of co-active neuronal populations. These observations suggest that a low tone of ACh controls the timing of neuronal co-activation during Up and Down states in the mEC, which might affect the hippocampal-neocortical information flow during SWS.

Low physiological concentrations of ACh prolong Up states and increase their occurrence via muscarinic receptor activation

We investigated how submicromolar concentrations of ACh affect the Up-Down state activity in the mEC. We found that ACh increases the duration of individual Up states as well as their incidence via muscarinic receptor activation (Figure 1) as previously reported in the neocortex (Carracedo *et al.*, 2013). We did not observe any effect of nicotinic receptor blockers on the ACh-induced modulation of Up and Down states. This is to be expected since most nicotinic receptors have an affinity for ACh in the micromolar range while α7 homomeric receptors, the only nicotinic receptors expressed in the cortex with submicromolar affinity for ACh, show fast desensitization (Christophe *et al.*, 2002; Hay *et al.*, 2015, 2016). Of the 5 sub-families of muscarinic receptors (M1 to M5), which all have submicromolar affinities for ACh (Levey, 1996; Lucas-Meunier *et al.*, 2003; Brown, 2010), we found that both sub-families M1/M3 and M2/M4 receptors may contribute to the cholinergic modulation of Up state activity. An M1/M3 receptor blocker almost fully abolished ACh-induced Up state modulation while an M2/M4 receptor blocker affected Up state incidence but not their duration (Figure 2). M1/M3 receptors show apparently opposing effects on mEC neurons: they depolarise principal neurons and increase their excitability, but suppress excitatory synaptic transmission (Klink & Alonso, 1997; Richter *et al.*, 1999; Yun *et al.*, 2000; Cheong *et al.*, 2001; Egorov *et al.*, 2002; Hamam *et al.*, 2007; Barrett & Chapman, 2013). We observed a decrease in the excitatory synaptic charge transfer in the presence of ACh, consistent with a suppression of excitatory transmission by the activation of M1/M3 receptors (Figure 3). The concomitant decrease in inhibitory synaptic charge transfer could be due to the reduced recurrent excitatory input coupled with the activation of M2/M4 receptors, which are G_i-coupled (Levey *et al.*, 1991; Levey, 1996; Chaudhuri *et al.*, 2005; Bubser *et al.*, 2012). The net effect was an increase in Up state duration and incidence (Figures 1 and 2), which suggests that the network response to muscarinic receptor activation is mediated primarily through the depolarisation of excitatory neurons.

Whereas we report an increase in Up state duration coupled with a doubling of Up state occurrence in the presence of submicromolar concentrations of ACh, at a higher concentration (5 μM), we observed a switch from Up and Down states to slow sinusoidal-like oscillations, similar to those observed in layer II stellate cells upon depolarisation (Dickson et al., 2000). The lengthening of Up states and shortening of Down states with low concentrations of ACh are consistent with another recent report in entorhinal cortex, which used carbachol in submicromolar concentrations (Nghiem *et al.*, 2020). However, the effect of higher concentrations of ACh differs somewhat from what was reported in the neocortex. In thalamocortical slices, Wester and Contreras reported that 100 μM ACh increased Up state incidence with no effect on Up state duration, whereas 1 mM ACh reduced Up state duration (Wester & Contreras, 2013), whereas Favero et al. reported that 5 μM of the cholinergic agonist carbachol abolished Up states

altogether (Favero *et al.*, 2012). The balance of synaptic suppression and direct activation of principal neurons by M1/M3 receptor activation at different ACh concentrations may explain the somewhat different results in the mEC and neocortex.

Our study revealed an increase in Up state duration in neurons recorded in current clamp mode (Figure 1), but no change in duration of Up state-associated synaptic activity in voltage-clamp mode (Figure 3). Several mechanisms may contribute to this apparent discrepancy. First, neurons with broadened spiking periods may not have been as strongly recurrently connected to the network involved in the Up states. This might explain how the increased spiking activity seen in the period immediately preceding synaptic Up states did not produce synaptic currents (Figure 4). However, it is unclear whether this is due to an anatomical lack of recurrent connectivity or a cholinergically induced change in functional connectivity through activation of presynaptic inhibitory muscarinic receptors. Additionally, some neurons may display frequency depression of synaptic transmission onto their postsynaptic targets, and it is also possible that the increase in Up state duration in current clamp in some neurons results from the activation of a cholinergically-induced intrinsic plateau potential (Egorov et al., 2002; Klink and Alonso, 1997), without the occurrence of action potentials in the later part of the Up-state-associated depolarisation, thus explaining the paucity of synaptic events towards the end of Up states (Figure 1).

Action potential discharge across Up and Down states

Our cell-attached recordings indicate that around 50% of the neurons increase their firing rate in response to a low concentration of ACh while 50% show a decrease (Figure 5). This result might appear surprising since we observed an increase in Up state duration and incidence (Figures 1 and S1-1). Nevertheless, the proportion of neurons showing an increase in spiking activity is consistent with the proportion of neurons (30-100%) that shows sustained activity in response to cholinergic activation in the presence of glutamate and GABA receptor blockers (Tahvildari *et al.*, 2008; Jochems *et al.*, 2013; Batallán-Burrowes & Chapman, 2018). Thus, it is plausible that muscarinic receptor-induced depolarisation in neurons expressing M1/M3 receptors leads to the observed increase in firing. In contrast, in neurons that show less expression of M1/M3 receptors, the combination of synaptic suppression and reduced spiking activity in 50% of neurons might reduce synaptic excitation and lead to a decrease in firing rate.

Up states are network events characterised by an increase in neuronal and synaptic activity (Steriade, McCormick, *et al.*, 1993; Steriade, Nunez, *et al.*, 1993). Our understanding of Up and Down states comes mainly from recordings made in anaesthetised animals and whole-cell recordings in slices. In anaesthetised animals, the majority of action potential discharges occur during Up states (Saleem *et al.*, 2010) but most anaesthetics are associated with low activity of modulatory neurons, including basal forebrain cholinergic neurons (Manns *et al.*, 2003). This might explain why action potential discharge during Down states is infrequently reported in anaesthetised preparations. Moreover, previously published studies often defined Up state boundaries using multi-unit activity as a marker of Up state, limiting the possibility to appreciate firing during Down states (see, for example, Jercog *et al.*, 2017). Whilst GABAergic interneurons display firing activity during Down states (Zucca *et al.*, 2019), further investigation in naturally-sleeping animals would be required to investigate to what extent cortical principal neurons fire during Down states.

Correspondence between population events and Up states

We used calcium imaging to study neuronal activity during population events (Figures 5-8), which we defined as peaks in the mean fluorescence changes across neurons. Because the change in GCaMP6f fluorescence is primarily caused by action potentials (Chen *et al.*, 2013), and neurons in our slice preparation predominantly fire during Up states (Figure 4), we surmised that population events correspond to electrophysiologically defined Up states. This correspondence was visible in the elevated $\Delta F/F_0$ signal during simultaneously recorded calcium transients and electrophysiological Up states (Figure 5). However, the electrophysiologically recorded Up states were twice as frequent as the population events while their duration was comparable (Figures 1 and 5). This difference in apparent incidence could be explained if some Up states are associated with firing of a too small number of neurons to give a population mean signal that is detected as a population event. This is particularly the case in control conditions where neurons showed low firing rates and thus likely small fluorescence changes. Moreover, we were technically constrained to low acquisition rates (<3 Hz), which might have limited our capability of capturing the calcium fluorescence peaks. Muscarinic receptor activation was reported to amplify the calcium rise from intracellular stores in response to a train of action potentials (Power & Sah, 2002). This effect might explain the observed increase in amplitude of fluorescence changes in the presence of ACh (Figure 6D); however, it should not affect the reported frequency or duration of the population events. Thus, even with some technical differences between the two sets of

experiments, we feel confident that the Up states recorded at single cell level using the patch-clamp technique and the population calcium events observed using two-photon microscopy reflect the same network events.

ACh increases synchronised periodic activity and reorganises network activity

Up and Down state transitions correspond to the alternation between synchronous population events and quiescent periods. The synchronous activity of regular periodicity gave rise to significant non-zero-lag peaks in the autocorrelation (Figure 7) with a period corresponding to the population event incidence. A similar increase in the periodicity of Up states was reported by muscarinic receptor activation in sensory cortices (Carracedo *et al.*, 2013; Lőrincz *et al.*, 2015). We observed that the population events reliably recruited the same assembly of cells throughout the duration of the recording (Figure 8A). ACh reorganised the active network with some cells reversibly dropping out and others reversibly joining the active assembly (Figure 8B). At the individual cell level, this change was reflected by an increase in activity of some cells and a decrease in others (Figure 4C,H). It is conceivable that the combination of intrinsic depolarisation and excitatory synaptic suppression induced by ACh would favour neurons that are part of assemblies with strong synaptic interconnectivity, allowing the induction of cholinergic persistent activity in these cells while reducing the recurrent excitation that weaker assemblies would receive. This mechanism could promote spiking contrast between sets of neuronal assemblies.

Conclusion

We found that ACh increases Up state duration and modulates spiking activity in principal neurons of the mEC. As the main gateway between the hippocampus and the neocortex, the mEC Up states may control the degree of coupling between the hippocampus and the neocortex (Hahn *et al.*, 2012). Therefore, because the level of ACh varies during SWS (Jing *et al.*, 2019), the cholinergic modulation of Up state duration in the mEC could serve as a mechanism to modulate the degree of coupling between the hippocampus and neocortex during SWS, and thereby influence memory consolidation (Tonegawa *et al.*, 2015; van de Ven *et al.*, 2016). More research would be needed to establish to what extent ACh has a role in the modulation of this coupling.

Acknowledgements: We are grateful to Drs Adam Hantman and Joshua Dudman at the Janelia Research Campus for providing Necab1-cre mice. We would like to thank Dr Melodie Borel for her help on Igor script analysis and Dr Michael T. Craig for the automated Up-Down state analysis. V.M. was initially supported by a Swiss National Science Foundation Early Postdoc Mobility Fellowship. This research was supported by the Biotechnology and Biological Sciences Research Council, U.K.

Competing interests: The authors declare no competing financial interests.

Author contributions: YAH, RD, VB and VM performed electrophysiological recordings. YAH and YZ performed two-photon calcium imaging experiments. YAH, PJ, YZ and VM analysed the data. YAH, PJ, OP and VM wrote the manuscript.

Data availability statement: Code used for the analysis of electrophysiological and calcium imaging data and to generate the figures can be accessed on the authors' GitHub site: https://github.com/przemyslawj/ento_ach_caimg. Electrophysiological and calcium imaging data will be shared on any reasonable request.

Abbreviations:

ACh: acetylcholine

aCSF: artificial cerebrospinal fluid

Atr: Atropine

FOV: field of view

mEC: medial entorhinal cortex

mec: mecamylamine

Pir: Pirenzepine

ROI: region of interest

SWS: Slow wave sleep

References:

Alcami, P., Franconville, R., Llano, I., & Marty, A. (2012) Measuring the firing rate of high-resistance neurons with cell-attached recording. *J. Neurosci.*, **32**, 3118–3130.

Barrett, S.G. & Chapman, C.A. (2013) Contribution of muscarinic M1 receptors to the cholinergic suppression of synaptic responses in layer II of the entorhinal cortex. *Neurosci. Lett.*, **554**, 11–15.

Batallán-Burrowes, A.A. & Chapman, C.A. (2018) Dopamine suppresses persistent firing in layer III lateral entorhinal cortex neurons. *Neurosci. Lett.*, **674**, 70–74.

Brown, D.A. (2010) Muscarinic Acetylcholine Receptors (mAChRs) in the Nervous System: Some Functions and Mechanisms. *J. Mol. Neurosci.*, **41**, 340–346.

Bubser, M., Byun, N., Wood, M.R., & Jones, C.K. (2012) Muscarinic receptor pharmacology and circuitry for the modulation of cognition. In Fryer, A.D., Christopoulos, A., & Nathanson, N.M. (eds), *Muscarinic Receptors*. Springer Berlin Heidelberg, Berlin, Heidelberg, pp. 121–166.

Carracedo, L.M., Kjeldsen, H., Cunnington, L., Jenkins, A., Schofield, I., Cunningham, M.O., Davies, C.H., Traub, R.D., & Whittington, M.A. (2013) A neocortical delta rhythm facilitates reciprocal interlaminar interactions via nested theta rhythms. *J. Neurosci.*, **33**, 10750–10761.

Chaudhuri, J.D., Hiltunen, M., Nykänen, M., Ylä-Herttuala, S., Soininen, H., & Miettinen, R. (2005) Localization of m2 muscarinic receptor protein in parvalbumin and calretinin containing cells of the adult rat entorhinal cortex using two complementary methods. *Neuroscience*, **131**, 557–566.

Chen, T.-W., Wardill, T.J., Sun, Y., Pulver, S.R., Renninger, S.L., Baohan, A., Schreiter, E.R., Kerr, R.A., Orger, M.B., Jayaraman, V., Looger, L.L., Svoboda, K., & Kim, D.S. (2013) Ultrasensitive fluorescent proteins for imaging neuronal activity. *Nature*, **499**, 295–300.

Cheong, M.Y., Yun, S.H., Mook-Jung, I., Joo, I., Huh, K., & Jung, M.W. (2001) Cholinergic modulation of synaptic physiology in deep layer entorhinal cortex of the rat. *J. Neurosci. Res.*, **66**, 117–121.

Christophe, E., Roebuck, A., Staiger, J.F., Lavery, D.J., Charpak, S., & Audinat, E. (2002) Two types of nicotinic receptors mediate an excitation of neocortical layer I interneurons. *J. Neurophysiol.*, **88**, 1318–1327.

Craig, M.T., Mayne, E.W., Bettler, B., Paulsen, O., & McBain, C.J. (2012) Distinct roles of $GABA_{B1a}$- and $GABA_{B1b}$-containing $GABA_B$ receptors in spontaneous and evoked termination of persistent cortical activity. *J. Physiol.,* **591**, 835–843.

Dana, H., Chen, T.-W., Hu, A., Shields, B.C., Guo, C., Looger, L.L., Kim, D.S., & Svoboda, K. (2014) Thy1-GCaMP6 transgenic mice for neuronal population imaging in vivo. *PLOS ONE*, **9**, e108697.

Dickson, C.T., Magistretti, J., Shalinsky, M.H., Fransén, E., Hasselmo, M.E., & Alonso, A. (2000) Properties and role of I(h) in the pacing of subthreshold oscillations in entorhinal cortex layer II neurons. *J. Neurophysiol.*, **83**, 2562–2579.

Digby, R.J., Bravo, D.S., Paulsen, O., & Magloire, V. (2017) Distinct mechanisms of Up state maintenance in the medial entorhinal cortex and neocortex. *Neuropharmacology*, **113**, 543–555.

Egorov, A.V., Hamam, B.N., Fransén, E., Hasselmo, M.E., & Alonso, A.A. (2002) Graded persistent activity in entorhinal cortex neurons. *Nature*, **420**, 173–178.

Favero, M., Varghese, G., & Castro-Alamancos, M.A. (2012) The state of somatosensory cortex during neuromodulation. *J. Neurophysiol.*, **108**, 1010–1024.

Fransén, E., Tahvildari, B., Egorov, A.V., Hasselmo, M.E., & Alonso, A.A. (2006) Mechanism of graded persistent cellular activity of entorhinal cortex layer V neurons. *Neuron*, **49**, 735–746.

Hahn, T.T.G., McFarland, J.M., Berberich, S., Sakmann, B., & Mehta, M.R. (2012) Spontaneous persistent activity in entorhinal cortex modulates cortico-hippocampal interaction in vivo. *Nat. Neurosci*. **15**, 1531–1538.

Hájos, N., Ellender, T.J., Zemankovics, R., Mann, E.O., Exley, R., Cragg, S.J., Freund, T.F., & Paulsen, O. (2009) Maintaining network activity in submerged hippocampal slices: importance of oxygen supply. *Eur. J. Neurosci.*, **29**, 319–327.

Hamam, B.N., Sinai, M., Poirier, G., & Chapman, C.A. (2007) Cholinergic suppression of excitatory synaptic responses in layer II of the medial entorhinal cortex. *Hippocampus*, **17**, 103–113.

Hasselmo, M.E. & McGaughy, J. (2004) High acetylcholine levels set circuit dynamics for attention and encoding and low acetylcholine levels set dynamics for consolidation. *Prog. Brain Res.,* **145***,* 207–231.

Hay, Y.A., Andjelic, S., Badr, S., & Lambolez, B. (2015) Orexin-dependent activation of layer VIb enhances cortical network activity and integration of non-specific thalamocortical inputs. *Brain Struct. Funct.*, **220**, 3497–3512.

Hay, Y.A., Lambolez, B., & Tricoire, L. (2016) Nicotinic transmission onto layer 6 cortical neurons relies on synaptic activation of non-α7 receptors. *Cereb. Cortex*, **26**, 2549–2562.

Jercog, D., Roxin, A., Barthó, P., Luczak, A., Compte, A., & de la Rocha, J. (2017) UP-DOWN cortical dynamics reflect state transitions in a bistable network. *eLife*, **6**, e22425.

Jing, M., Li, Y., Zeng, J., Huang, P., Skirzewski, M., Kljakic, O., Peng, W., Qian, T., Tan, K., Wu, R., Zhang, S., Pan, S., Xu, M., Li, H., Saksida, L.M., Prado, V.F., Bussey, T., Prado, M.A.M., Chen, L., Cheng, H., & Li, Y. (2019) An optimized acetylcholine sensor for monitoring in vivo cholinergic activity. *bioRxiv*, 861690.

Jochems, A., Reboreda, A., Hasselmo, M.E., & Yoshida, M. (2013) Cholinergic receptor activation supports persistent firing in layer III neurons in the medial entorhinal cortex. *Behav. Brain Res.*, **254**, 108–115.

Kametani, H. & Kawamura, H. (1990) Alterations in acetylcholine release in the rat hippocampus during sleep-wakefulness detected by intracerebral dialysis. *Life Sci.*, **47**, 421–426.

Klink, R. & Alonso, A. (1997) Ionic mechanisms of muscarinic depolarization in entorhinal cortex layer II neurons. *J. Neurophysiol.*, **77**, 1829–1843.

Lee, M.G., Hassani, O.K., Alonso, A., & Jones, B.E. (2005) Cholinergic basal forebrain neurons burst with theta during waking and paradoxical sleep. *J. Neurosci.*, **25**, 4365–4369.

Levey, A.I. (1996) Muscarinic acetylcholine receptor expression in memory circuits: implications for treatment of Alzheimer disease. *Proc. Natl. Acad. Sci. U. S. A.*, **93**, 13541–13546.

Levey, A.I., Kitt, C.A., Simonds, W.F., Price, D.L., & Brann, M.R. (1991) Identification and localization of muscarinic acetylcholine receptor proteins in brain with subtype-specific antibodies. *J. Neurosci.*, **11**, 3218–3226.

Lőrincz, M.L., Gunner, D., Bao, Y., Connelly, W.M., Isaac, J.T.R., Hughes, S.W., & Crunelli, V. (2015) A distinct class of slow (~0.2–2 Hz) intrinsically bursting layer 5 pyramidal neurons determines UP/DOWN state dynamics in the neocortex. *J. Neurosci.*, **35**, 5442–5458.

Lucas-Meunier, E., Fossier, P., Baux, G., & Amar, M. (2003) Cholinergic modulation of the cortical neuronal network. *Pflugers Arch.*, **446**, 17–29.

Madisen, L., Garner, A.R., Shimaoka, D., Chuong, A.S., Klapoetke, N.C., Li, L., van der Bourg, A., Niino, Y., Egolf, L., Monetti, C., Gu, H., Mills, M., Cheng, A., Tasic, B., Nguyen, T.N., Sunkin, S.M., Benucci, A., Nagy, A., Miyawaki, A., Helmchen, F., Empson, R.M., Knöpfel, T., Boyden, E.S., Reid, R.C., Carandini, M., & Zeng, H. (2015) Transgenic mice for intersectional targeting of neural sensors and effectors with high specificity and performance. *Neuron*, **85**, 942–958.

Mann, E.O., Kohl, M.M., & Paulsen, O. (2009) Distinct roles of $GABA_A$ and $GABA_B$ receptors in balancing and terminating persistent cortical activity. *J. Neurosci.*, **29**, 7513–7518.

Manns, I.D., Alonso, A., & Jones, B.E. (2003) Rhythmically discharging basal forebrain units comprise cholinergic, GABAergic, and putative glutamatergic cells. *J. Neurophysiol.*, **89**, 1057–1066.

Marrosu, F., Portas, C., Mascia, M.S., Casu, M.A., Fà, M., Giagheddu, M., Imperato, A., & Gessa, G.L. (1995) Microdialysis measurement of cortical and hippocampal acetylcholine release during sleep-wake cycle in freely moving cats. *Brain Res.*, **671**, 329–332.

Mena-Segovia, J., Sims, H.M., Magill, P.J., & Bolam, J.P. (2008) Cholinergic brainstem neurons modulate cortical gamma activity during slow oscillations. *J. Physiol.*, **586**, 2947–2960.

Nghiem, T.-A.E., Tort-Colet, N., Górski, T., Ferrari, U., Moghimyfiroozabad, S., Goldman, J.S., Teleńczuk, B., Capone, C., Bal, T., di Volo, M., & Destexhe, A. (2020)

Cholinergic switch between two types of slow waves in cerebral cortex. *Cereb. Cortex*, **30**, 3451–3466.

Pachitariu, M., Stringer, C., Dipoppa, M., Schröder, S., Rossi, L.F., Dalgleish, H., Carandini, M., & Harris, K.D. (2017) Suite2p: beyond 10,000 neurons with standard two-photon microscopy. *bioRxiv*, 061507.

Parikh, V., Kozak, R., Martinez, V., & Sarter, M. (2007) Prefrontal acetylcholine release controls cue detection on multiple timescales. *Neuron*, **56**, 141–154.

Phillips, J.W., Schulmann, A., Hara, E., Winnubst, J., Liu, C., Valakh, V., Wang, L., Shields, B.C., Korff, W., Chandrashekar, J., Lemire, A.L., Mensh, B., Dudman, J.T., Nelson, S.B., & Hantman, A.W. (2019) A repeated molecular architecture across thalamic pathways. *Nat. Neurosci.*, **22**, 1925–1935.

Power, J.M. & Sah, P. (2002) Nuclear calcium signaling evoked by cholinergic stimulation in hippocampal CA1 pyramidal neurons. *J. Neurosci.*, **22**, 3454–3462.

Richter, M., Schilling, T., & Müller, W. (1999) Muscarinic control of intracortical connections to layer II in rat entorhinal cortex slice. *Neurosci. Lett.*, **273**, 200–202.

Saleem, A.B., Chadderton, P., Apergis-Schoute, J., Harris, K.D., & Schultz, S.R. (2010) Methods for predicting cortical UP and DOWN states from the phase of deep layer local field potentials. *J. Comput. Neurosci.*, **29**, 49–62.

Steriade, M. (2004) Acetylcholine systems and rhythmic activities during the waking–sleep cycle. *Prog. Brain Res.*, **145**, 179–196.

Steriade, M., McCormick, D.A., & Sejnowski, T.J. (1993) Thalamocortical oscillations in the sleeping and aroused brain. *Science*, **262**, 679–685.

Steriade, M., Nunez, A., & Amzica, F. (1993) A novel slow (< 1 Hz) oscillation of neocortical neurons in vivo: depolarizing and hyperpolarizing components. *J. Neurosci.*, **13**, 3252–3265.

Strien, N.M. van, Cappaert, N.L.M., & Witter, M.P. (2009) The anatomy of memory: an interactive overview of the parahippocampal–hippocampal network. *Nat. Rev. Neurosci.*, **10**, 272–282.

Tahvildari, B., Alonso, A.A., & Bourque, C.W. (2008) Ionic basis of on and off persistent activity in layer III lateral entorhinal cortical principal neurons. *J. Neurophysiol.*, **99**, 2006–2011.

Tonegawa, S., Liu, X., Ramirez, S., & Redondo, R. (2015) Memory engram cells have come of age. *Neuron*, **87**, 918–931.

van de Ven, G.M., Trouche, S., McNamara, C.G., Allen, K., & Dupret, D. (2016) Hippocampal offline reactivation consolidates recently formed cell assembly patterns during sharp wave-ripples. *Neuron*, **92**, 968–974.

Wester, J.C. & Contreras, D. (2013) Differential modulation of spontaneous and evoked thalamocortical network activity by acetylcholine level in vitro. *J. Neurosci.*, **33**, 17951–17966.

Yun, S.H., Cheong, M.Y., Mook-Jung, I., Huh, K., Lee, C.-J., & Jung, M.W. (2000) Cholinergic modulation of synaptic transmission and plasticity in entorhinal cortex and hippocampus of the rat. *Neuroscience*, **97**, 671–676.

Zhang, H., Lin, S.-C., & Nicolelis, M.A.L. (2010) Spatiotemporal coupling between hippocampal acetylcholine release and theta oscillations in vivo. *J. Neurosci.*, **30**, 13431–13440.

Zhang, Z., Reboreda, A., Alonso, A., Barker, P.A., & Séguéla, P. (2011) TRPC channels underlie cholinergic plateau potentials and persistent activity in entorhinal cortex. *Hippocampus*, **21**, 386–397.

Zucca, S., Pasquale, V., Lagomarsino de Leon Roig, P., Panzeri, S., & Fellin, T. (2019) Thalamic drive of cortical parvalbumin-positive interneurons during down states in anesthetized mice. *Curr. Biol.*, **29**, 1481-1490.e6.

Figures captions

Figure 1: **Submicromolar ACh concentrations prolong Up state activity in the mEC via muscarinic receptor activation. A:** Example of whole-cell recording from layer III principal neuron in control condition and after 500 nM ACh and ACh + atropine (Atr, 1 µM) superfusion. **B-C:** Comparison of Up state duration and Up state incidence in (**B**) control, ACh and ACh + Atr conditions (n = 11) and (**C**) control, Atr and Atr + ACh conditions (n = 7). **D:** Example of whole-cell recording from layer III principal neuron in control condition and after 500 nM ACh and ACh + Mecamylamine (Mec, 10 µM) superfusion. **E-F:** Comparison of Up state duration and Up state incidence in (**E**) control, ACh and ACh + Mec conditions (n = 9) and in (**F**) control, Mec and Mec + ACh conditions (n = 7). * indicates $p < 0.05$.

Figure 2: **Submicromolar ACh concentrations prolong Up state activity via type 1/3 and 2/4 muscarinic receptor activation. A:** Example of whole-cell recording from layer III principal neuron in control condition and after 500 nM ACh and ACh + Pirenzepine (Pir, 10 µM) superfusion. **B-C:** Comparison of Up state duration and incidence in (**B**) control, ACh and ACh + Pir conditions (n = 7) and (**C**) control, Pir and Pir + ACh conditions (n = 6). **D:** Example of whole-cell recording from layer III principal neuron in control condition and after 500 nM ACh and ACh + AFDX-116 (AFDX, 1 µM) superfusion. **E-F:** Comparison of Up state duration and Up state incidence in (**E**) control, ACh and ACh + AFDX conditions (n = 7) and in (**F**) control, AFDX and AFDX + ACh conditions (n = 9). * indicates $p < 0.05$.

Figure 3: Effect of acetylcholine on excitatory and inhibitory synaptic transmission during Up states. A: Example of voltage-clamp recording of synaptic persistent activity before (black) and after bath application of 250-500 nM ACh (grey). Top, excitatory synaptic currents, holding potential -70 mV. Bottom, inhibitory synaptic currents, holding potential +10 mV. **B-E:** Plots showing (B) the charge transfer of excitatory and inhibitory currents, and (C) the ratio of excitation/inhibition (E/I ratio). Note that both excitatory and inhibitory synaptic transmission are significantly reduced by ACh in a proportional manner during Up states. Consequently, the E/I ratio is not affected by ACh (n = 9). (D) The estimated input resistance, and (E) the duration of excitatory and inhibitory synaptic Up state activity, * indicates $p < 0.05$.

Figure 4: Acetylcholine modulates spiking behaviour across Up and Down states. A: Dual voltage-clamp and cell-attached recordings in the mEC in the absence (black trace) or presence of 250-500 nM ACh (grey trace). Cell-attached recording shows spiking activity preferentially during synaptic Up state (grey shade) in control condition (black trace) which expands to Down state during application of ACh. **B:** Histograms representing the distribution of action potential discharges across Up and Down states for neuron in **A** in **Bi** and for the population of cells whose spike frequency increased in the presence of ACh in **Bii**. **C:** Example of a neuron that fired exclusively during Up state in control condition and with a decrease in spiking activity in the presence of ACh. **D:** Histograms representing the distribution of spikes across Up and Down states for neuron in **C** in **Di** and for the population of cells whose spike frequency decreased in the presence of ACh in **Dii**. **E:** Paired comparison of spike frequency in control and ACh conditions (n = 24). **F:** Quantification of spike frequency during Down and Up state in control and ACh conditions showing a significant increase in firing frequency by ACh in Down state (**Fi**) but not in Up state (**Fii**). **G:** Plot of change in spike frequency during Down state vs change in spike frequency during Up state, showing that some neurons increase their spike frequency during both Up and Down states (as shown in trace **A**), while other neurons decrease their spike frequency during Up state. **H:** Ratio of spike count during the first half of the Up state over the total spike count during the Up state. **I:** Distribution of firing frequency changes during Up states induced by ACh showing that the majority of layer III neurons increase their firing during Up states while layer II neurons on average decrease their firing. * indicates $p < 0.05$.

Figure 5: Calcium signal in individual cells correlates with electrophysiologically recorded Up states. A: Immunostaining from Necab-GCaMP6f and Thy1-GCaMP6f mice showing expression of GCaMP6f in mEC. **B:** Field of view showing seven cells (purple) from which calcium fluorescence was extracted and the patched cell filled with red dye (red). **C:** Simultaneous recording of the membrane potential of the red cell and the calcium fluorescence changes in the control and ACh (250 nM) conditions. Control and Acetylcholine panels represent calcium signals from the same 7 magenta cells shown in **B**. **D:** Cross-correlation between membrane potential of the electrophysiologically recorded cell and calcium fluorescence changes of the surrounding cells (Ctrl: n = 9 active neurons from 3 slices, ACh: n = 27 active neurons from 3 slices).

Figure 6: ACh increases synchrony in the network. A: The effect of ACh and atropine (Atr) application on population calcium activity. Top, $\Delta F/F_0$ signal. Middle, z-scored $\Delta F/F_0$ signal of all

cells from the same network during the Control, ACh, and ACh + Atr conditions. Activity of each cell is shown with a single horizontal line with colour coded z-score values. Bottom, mean population activity calculated in one-second time bins of the $\Delta F/F_0$ signal. Dashed line shows the threshold for detection of population events; events are marked by a red asterisk. **B:** Paired comparison of the population event durations between Ctrl and ACh conditions (n = 10), and between ACh and ACh + Atr conditions (n = 10). **C:** Paired comparison of the population event frequency between Ctrl and ACh conditions (n = 10) and between ACh and ACh + Atr (n = 10). **D:** Paired comparison of the median population event peaks between the Ctrl and ACh conditions (n = 10) and between ACh and ACh + Atr (n = 10). **E:** Change in frequency of calcium events after applying ACh. Cumulative distribution function of the difference between the cell mean event frequencies in the ACh and Ctrl conditions. Thin lines show distribution of changes in a single network; thick line shows the overall distribution with equal number of cells sampled from each network. Data included slices that had more than 10 cells active during the control condition. **F:** As in **E** but showing the ratio of calcium event durations during the ACh over the Ctrl condition.

Figure 7: ACh induces rhythmic activity in the network. A: Autocorrelation of the mean population activity from Figure 5D. Grey background shows 95% confidence interval for autocorrelations of a time series generated by a random moving average. Intervals were calculated with the Bartlett formula for the standard error estimate in a moving average model. **B:** Percent of the networks with significant autocorrelation for each recording condition. **C:** Periodicity in the network activity after applying ACh measured by the lag of the peak autocorrelation value. Data shown for significantly correlated networks (n = 8).

Figure 8: Population event recruitment and reversible modulation by ACh. A: Cumulative distribution function for the proportion of cells that participated in a given percentage of population events. The dashed vertical line marks the threshold for a population event-active cell – a cell participating in >70% of population events. A hundred of cells were sampled with repetition from each slice to make each slice contribute equally to the plotted distribution. **B:** Changes in the cell population participating in network events. The lines track how some cells changed from population event active to inactive and from inactive to active. The line thickness represents the relative fraction of cells that share the same pattern of activation across the three recording conditions. The dark grey lines track cells that returned to their previous state after atropine whether their activity changed by ACh or not. The light grey lines track cells that did not return to the previous activation state after atropine. The network reorganisation followed the atropine-

reversible pattern represented by dark grey lines, better than a model of random reassignments ($p < 0.01$, cells from all slices pooled together).

Figure S1-1: Submicromolar ACh concentrations increase Up state duration and incidence in the mEC. A-B: Examples of two whole-cell recordings from layer III principal neurons. A constant bias current was used to set the membrane potential at -70 mV at the start of the recording. **A** shows succession of control condition, bath application of 400 nM and 5 µM ACh and washout. Insets show Up states in control, during 400 nM ACh and after 15 min washout; Up state morphology is modified by ACh and does not wash out fully. **B** shows control and after application of 5 µM ACh. Insets show Up and Down states in control condition and the oscillating membrane potential during ACh application. **C-D:** Comparison of Up state duration (**C**) and incidence (**D**) at 100 nM (n = 5), 200 nM (n = 3), 300 nM (n = 3), 400 nM (n = 2) and 500 nM ACh (n = 8) indicates no significant difference in duration or incidence in this range of concentration.

Figure S6-1: Activity of all the slices imaged across the three recording conditions. z-scored $\Delta F/F_0$ signal of the cells from all different experiments shown during the Ctrl, ACh, and ACh + Atr conditions.

Figure 1

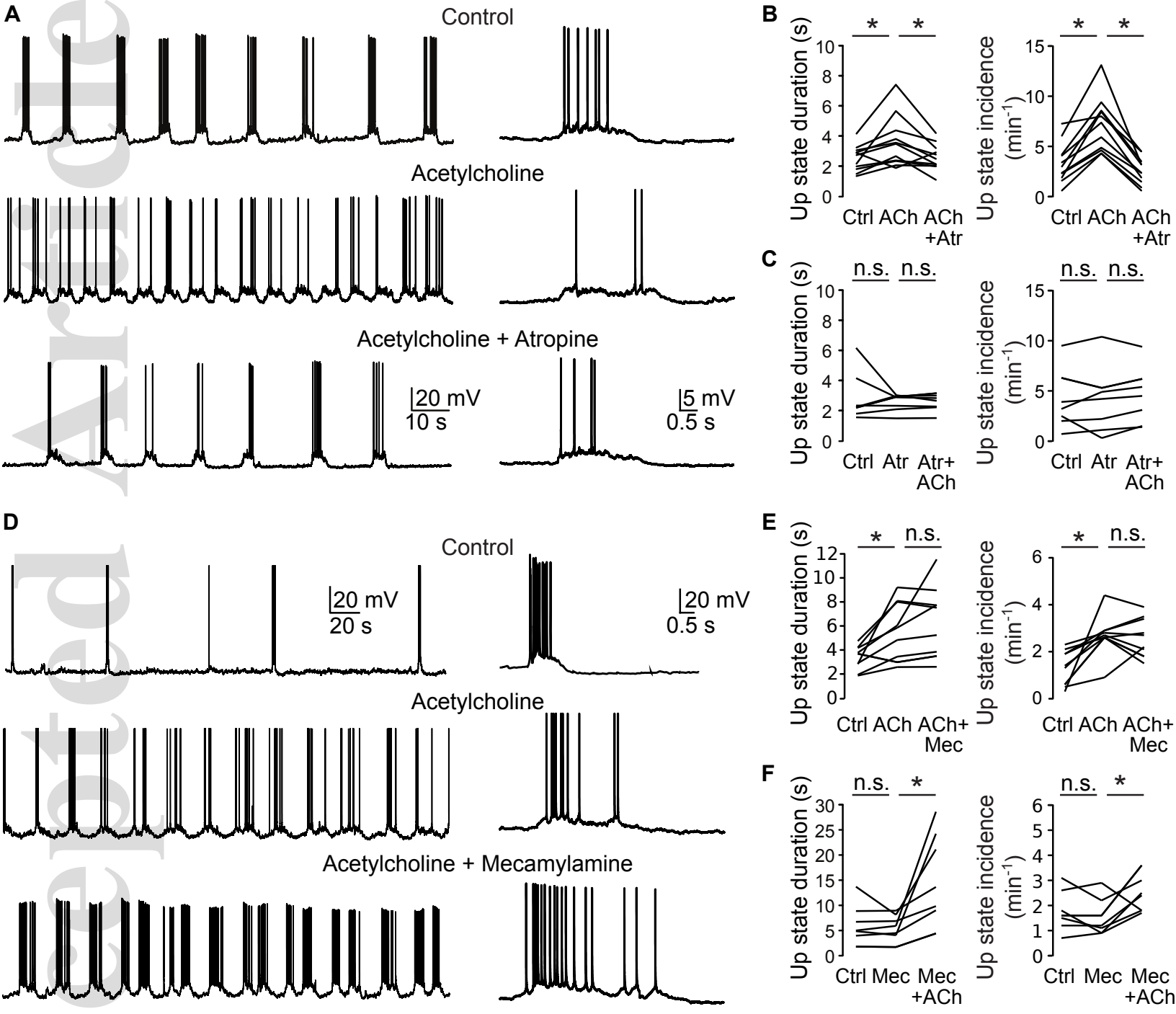

ejn_15032_f1.eps

Figure 2

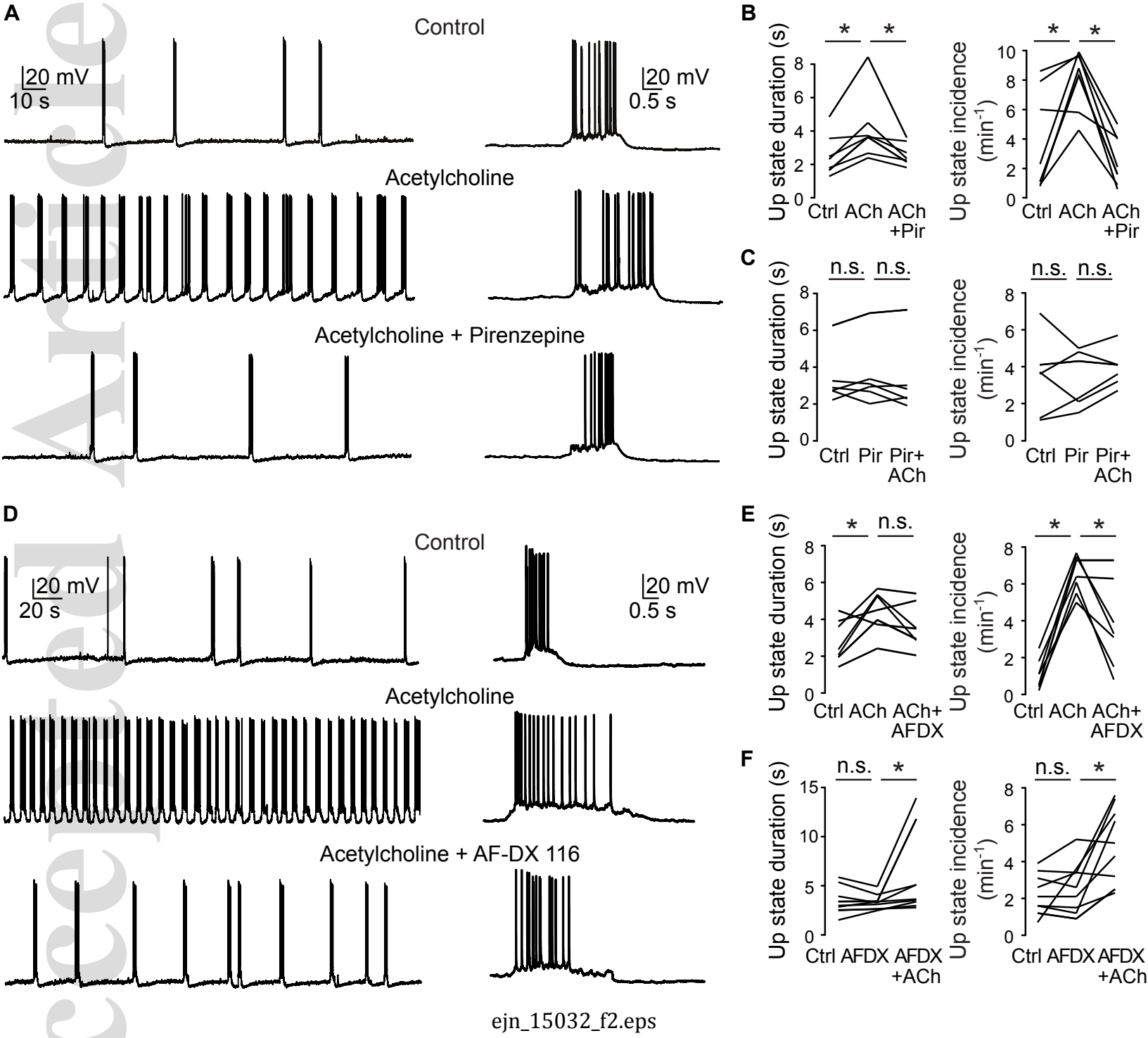

ejn_15032_f2.eps

Figure 3

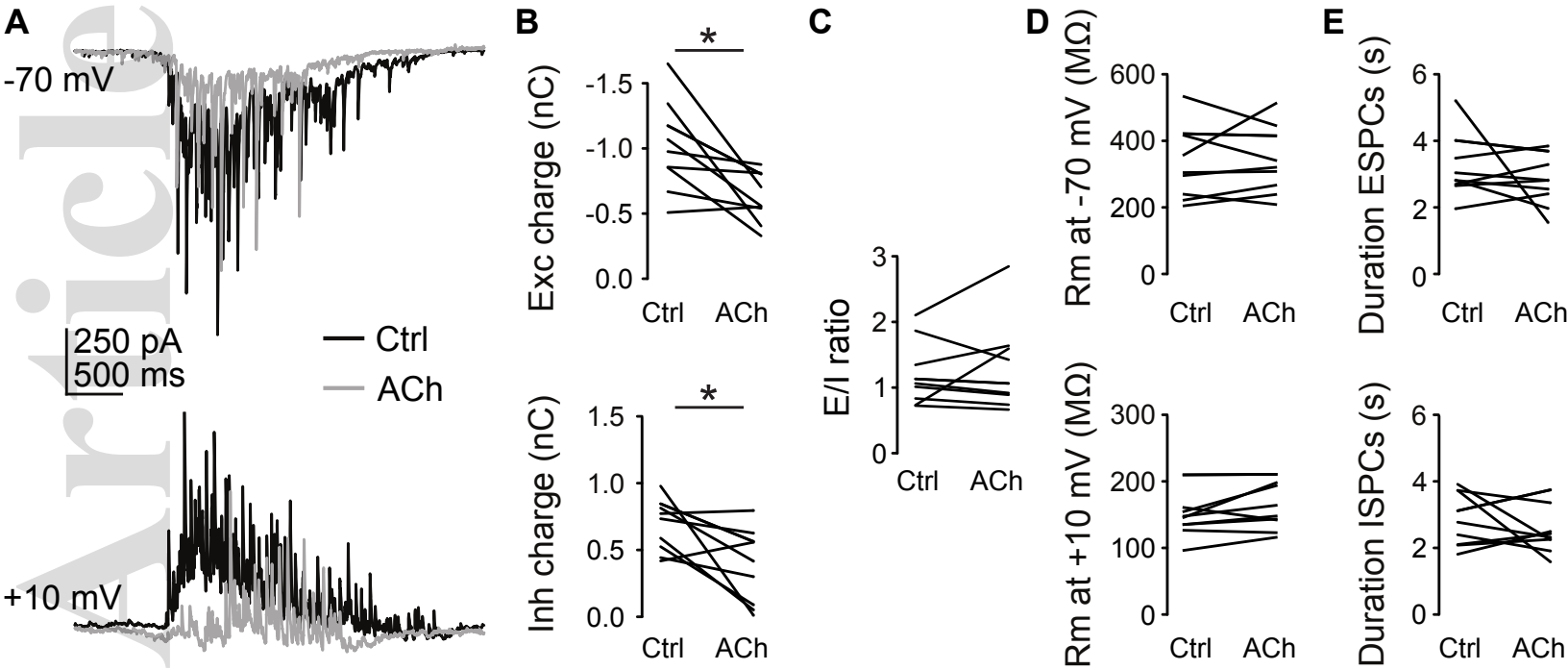

ejn_15032_f3.eps

Figure 4

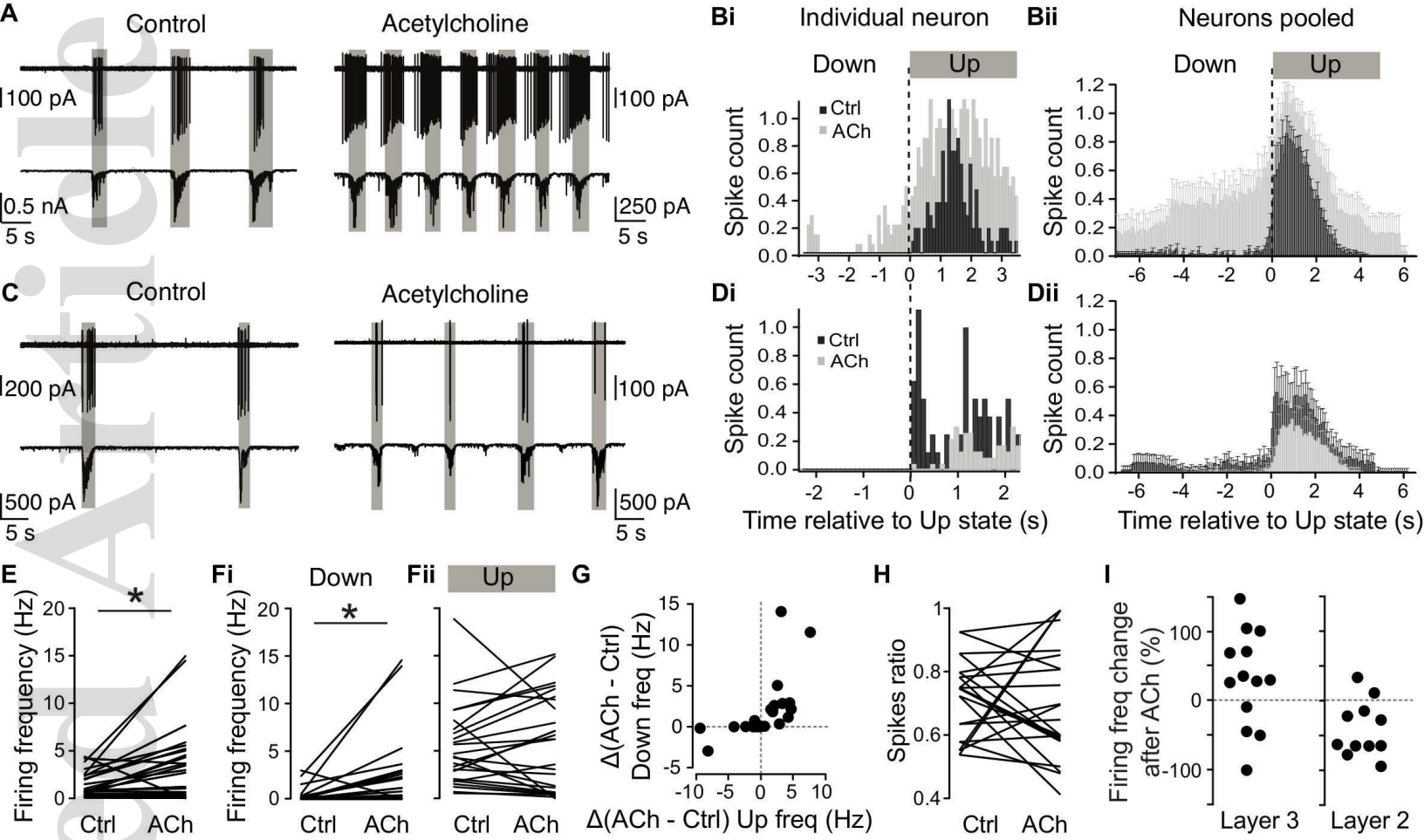

ejn_15032_f4.eps

Figure 5

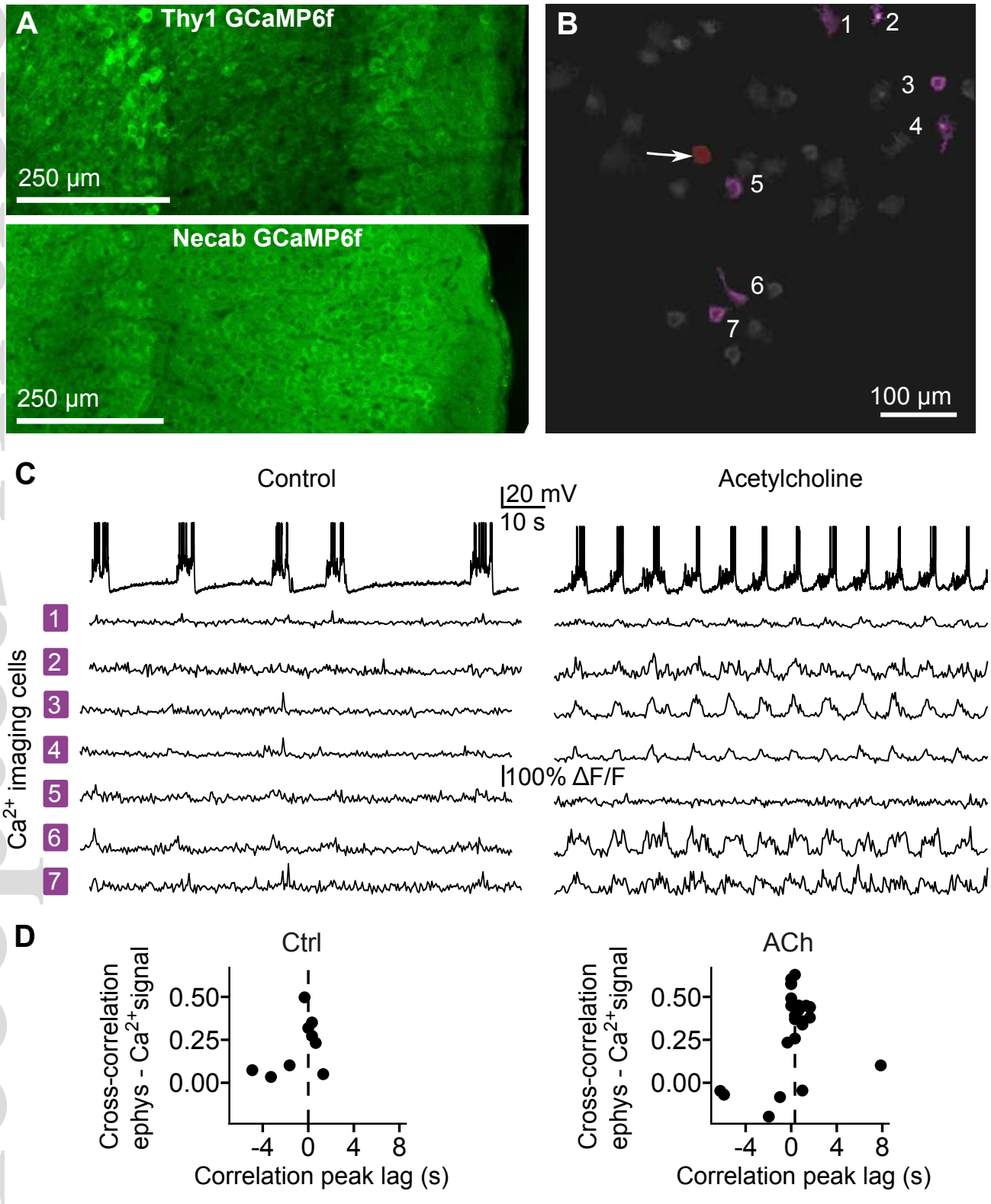

ejn_15032_f5.eps

Figure 6

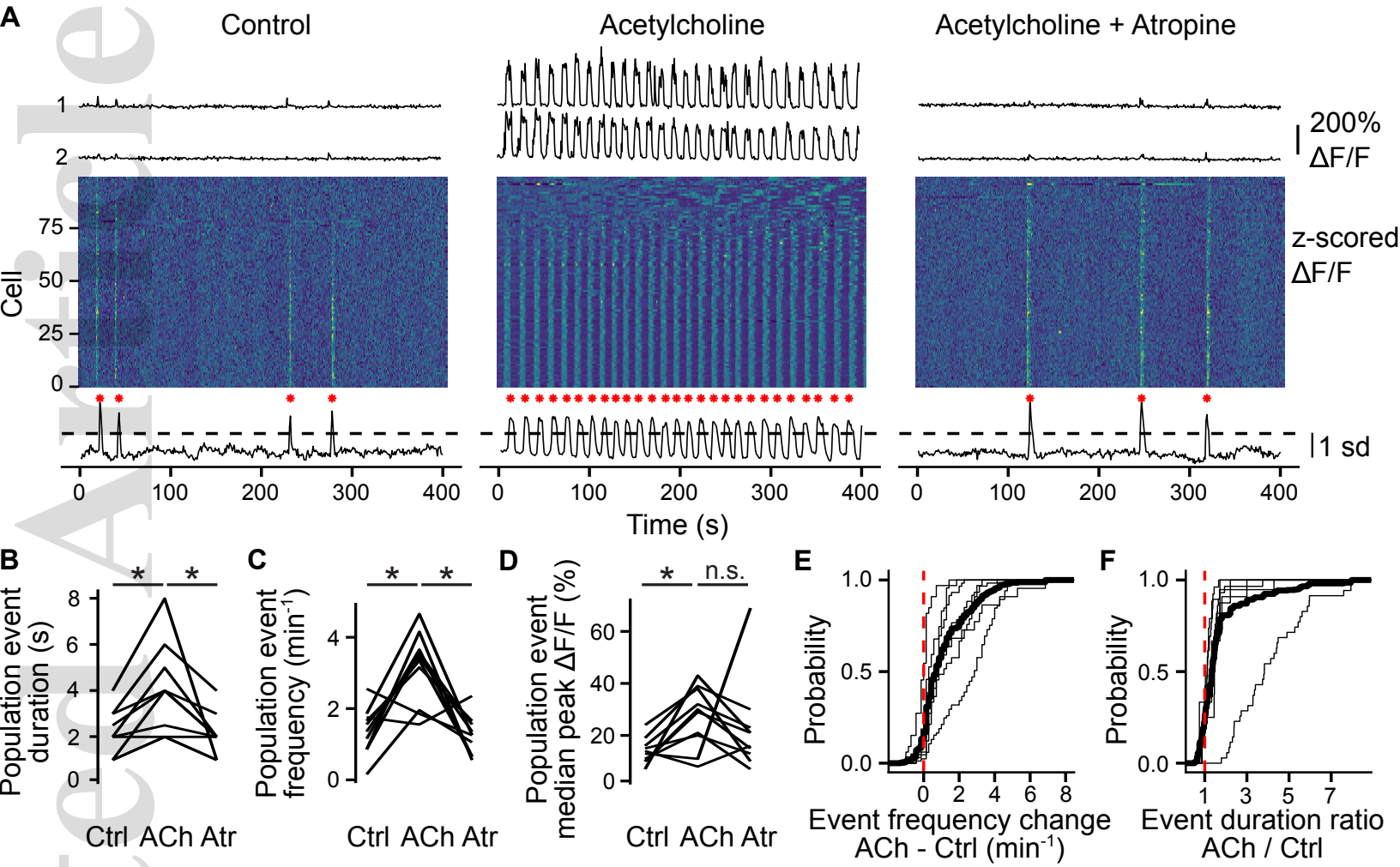

ejn_15032_f6.eps

Figure 7

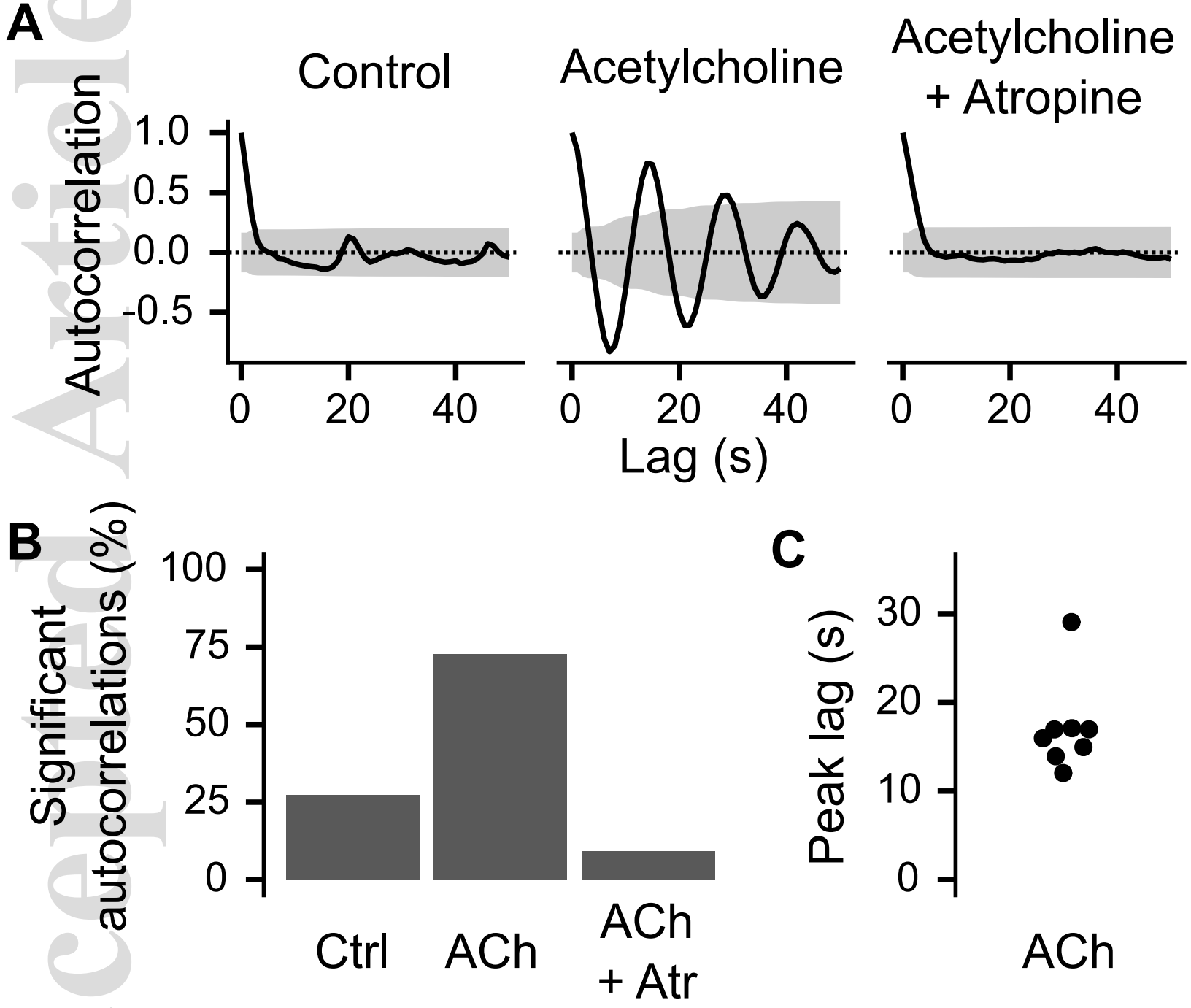

ejn_15032_f7.eps

Figure 8

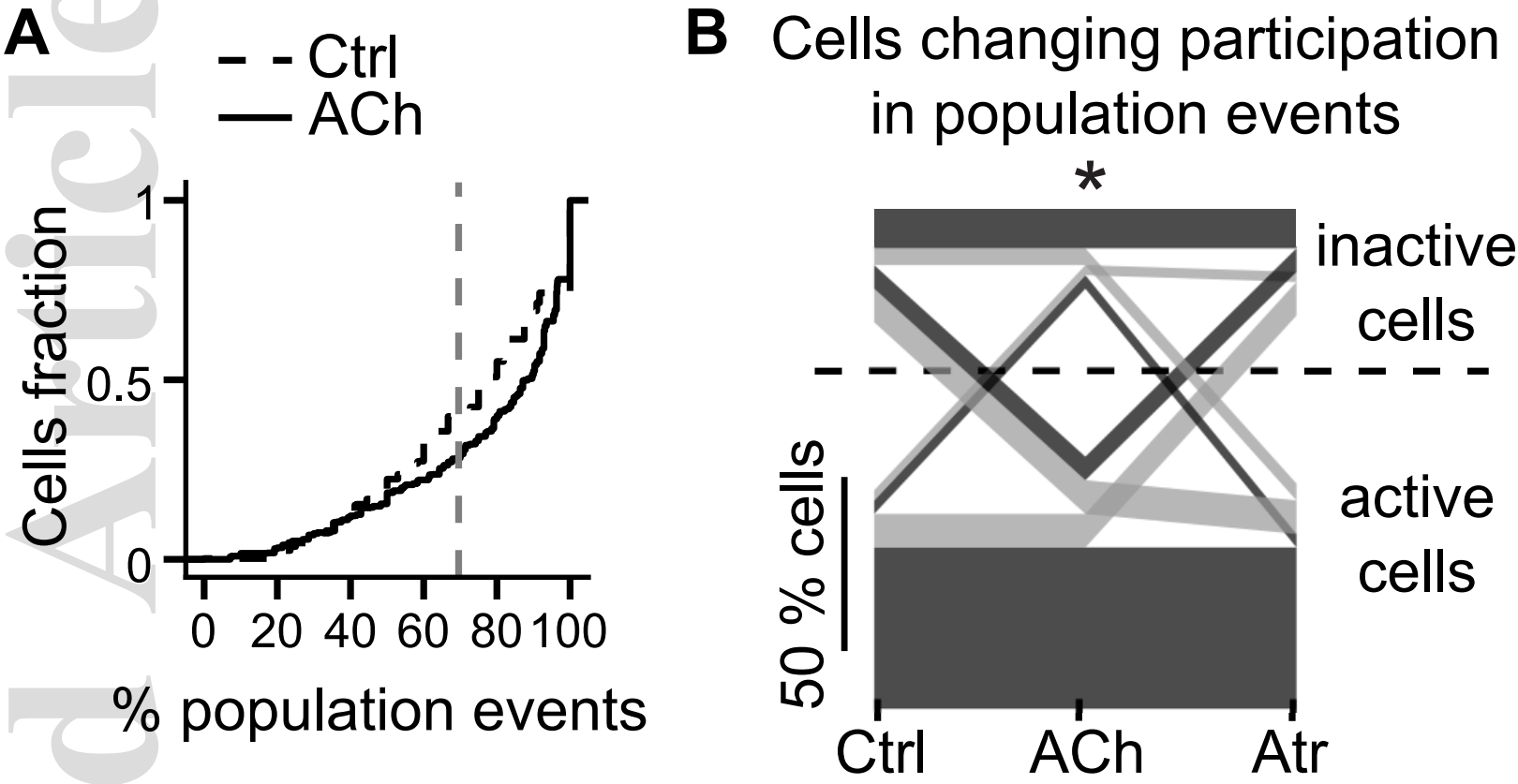

ejn_15032_f8.eps